https://doi.org/10.5194/egusphere-2022-806
Preprint. Discussion started: 19 September 2022

Use of machine learning to retrieve nitrogen dioxide with hyperspectral imagers in the ultraviolet and blue spectral range

Joanna Joiner[1], Sergey Marchenko[2], Zachary Fasnacht[2], Lok Lamsal[3], Can Li[4], Alexander Vasilkov[2], and Nickolay Krotkov[1]

[1]National Aeronautics and Space Administration, Goddard Space Flight Center, Laboratory for Atmospheric Chemistry and Dynamics, Code 614, Greenbelt, MD USA
[2]Science Systems and Applications, Inc., Lanham, MD USA
[3]University of Maryland, Baltimore County, MD USA
[4]University of Maryland, College Park, MD USA

Correspondence: Joanna Joiner(joanna.joiner@nasa.gov)

Abstract. Nitrogen dioxide (NO_2) is an important trace-gas pollutant and climate agent whose presence also leads to spectral interference in ocean color retrievals. NO_2 column densities have been retrieved with satellite UV-Vis spectrometers such as the Ozone Monitoring Instrument (OMI) and Tropospheric Monitoring Instrument (TROPOMI) that typically have spectral resolutions of the order of 0.5 nm or better and spatial footprints as small as 3.5 km $\times$ 5 km. These NO_2 observations are used to estimate emissions, monitor pollution trends, and study effects on human health. Here, we investigate whether it is possible to retrieve NO_2 amounts with lower spectral resolution hyper-spectral imagers such as the Ocean Color Instrument (OCI) that will fly on the Plankton, Aerosol, Cloud, ocean Ecosystem (PACE) satellite set for launch in early 2024. OCI will have a spectral resolution of 5 nm and a spatial resolution of $\sim$1 km with global coverage in 1-2 days. At this spectral resolution, small scale spectral structure from NO_2 absorption is still present. We use real spectra from the OMI to simulate OCI spectra that are in turn used to estimate NO_2 slant column densities (SCDs) with an artificial neural network trained on target OMI retrievals. While we obtain good results with no noise added to the OCI simulated spectra, we find that the expected instrumental noise substantially degrades the OCI NO_2 retrievals. Nevertheless, the NO_2 information from OCI may be of value for ocean color retrievals, as our simulations suggest that it will be of similar or slightly better quality as compared with TROPOMI NO_2 data at TROPOMI spatial resolution on a daily basis and will be available simultaneously. OCI retrievals can also be temporally averaged over time-scales of the order months to reduce noise and provide higher spatial resolution maps that may be useful for downscaling information provided by lower spatial resolution instruments such as OMI and TROPOMI, for high resolution emissions estimates, and other applications. In addition, we explore the possibility of using an extended fitting window for NO_2 retrievals as compared with traditional approaches. We demonstrate that the use of an extended spectral fitting window can reduce random errors in a current state-of-the-art OMI NO_2 SCD product. Machine learning approaches with extended fitting windows, once trained, can also substantially speed up NO_2 spectral fitting algorithms as applied to OMI, TROPOMI, and similar instruments that are flying or will soon fly in geostationary orbit.

https://doi.org/10.5194/egusphere-2022-806
Preprint. Discussion started: 19 September 2022

1 Introduction

Nitrogen dioxide (NO_2) is an important trace gas for both air quality and climate. It is identified as a criteria pollutant by the United States (US) Environmental Protection Agency (EPA). As a climate agent, it is a precursor for tropospheric ozone, a potent greenhouse gas in the upper troposphere. NO_2 also contributes in the formation of aerosols that can cool the planet by reflecting incoming solar radiation back to space (Shindell et al., 2009). Over non-polluted regions, most of the atmospheric column of NO_2 resides in the stratosphere where it participates in photochemical reactions that can affect the ozone layer (see e.g., van Geffen et al., 2020, and references therein).

Much effort has been expended to develop sophisticated physically-based retrieval algorithms for spectrometers that measure scattered solar radiation at ultraviolet (UV) and blue wavelengths at the ground (e.g., Noxon, 1975; Platt and Perner, 1983; Platt, 1994; Platt and Stutz, 2006) as well as from satellite platforms (e.g., Burrows et al., 1999; Richter and Burrows, 2002; Bucsela et al., 2006; Boersma et al., 2007, 2011; Valks et al., 2011; Bucsela et al., 2013; Yang et al., 2014; Marchenko et al., 2015; Boersma et al., 2018; van Geffen et al., 2020; Lamsal et al., 2021). Retrievals from satellite-based instruments such as the Global Ozone Monitoring Experiment (GOME) (Burrows et al., 1999), SCIAMACHY (Bovensmann et al., 1999), the Ozone Monitoring Experiment (OMI) (Levelt et al., 2006), GOME-2 (Munro et al., 2016), the Ozone Mapping and Profiler Suite - Nadir Mapper (OMPS-NM) (Bak et al., 2017), and the TROPOspheric Monitoring Experiment (TROPOMI) (Veefkind et al., 2012) have been used in numerous studies related to top-down emissions estimates, air quality monitoring and forecasting, pollution events, trends, and related health studies (see e.g., Bovensmann et al., 2011; Lamsal et al., 2015; Krotkov et al., 2016; Duncan et al., 2016; Levelt et al., 2018; Goldberg et al., 2021; Kerr et al., 2021; Cooper et al., 2022, and references therein).

NO_2 absorption impacts satellite radiance measurements that are used in ocean color algorithms. The affected spectral ranges include those used for retrievals of colored dissolved organic matter (CDOM) and chlorophyll-a (e.g., Mannino et al., 2008; Le and Hu, 2013). In particular, large variations in NO_2 total columns near polluted coastlines can affect ocean color measurements from sensors in both low Earth orbit (LEO) and Geostationary Earth Orbit (GEO) (Ahmad et al., 2007; Tzortziou et al., 2014). For example, under high NO_2 loading ($\sim 1 \times 10^{16}$ molec cm^{-2}), if not accounted for, errors in water leaving radiance could reach 10-20% (Ahmad et al., 2007) and produce spectral structure that can interfere with ocean color retrievals.

Two planned hyper-spectral imagers, the Ocean Color Instrument (OCI) on the Plankton, Aerosol, Cloud, ocean Ecosystem (PACE) mission in LEO and the GEO Geosynchronous Littoral Imaging and Monitoring Radiometer (GLIMR) were designed for ocean color measurements. The PACE OCI, scheduled to launch in the early 2024 time frame, will cover wavelengths from UV ($\sim$340 nm) through the short-wave infrared wavelengths. It will provide daily global coverage from LEO at a spatial resolution of approximately 1 km. GLIMR will make diurnal measurements at about 300 m spatial resolution over the Gulf of Mexico and surrounding coastlines later this decade (NASA, 2019). Use of a satellite-based NO_2 climatology, collocated satellite data from atmospheric instruments, such as TROPOMI, or simulated NO_2 from a chemistry transport model are all options for use in atmospheric correction algorithms for ocean property retrievals. However, all of these have shortcomings. For example, NO_2 derived from atmospheric instruments may not be available at the spatial or temporal scales of ocean color instruments. While a climatology or model simulations can capture the basic features of NO_2 including high values

https://doi.org/10.5194/egusphere-2022-806
Preprint. Discussion started: 19 September 2022

around coastal cities, they may miss important details of pollution plumes that can extend over the ocean. It should also be noted that while TROPOMI and PACE are in similar orbits (TROPOMI and PACE equator crossing times are 13:30 and 13:00, respectively), TROPOMI will be nearing its end of primary mission by the time PACE launches; its follow-on mission, Sentinel 5, will be in a morning orbit (09:30 equator crossing time) that will result in more temporal mismatch with PACE. Therefore, it has been a stated and challenging goal of these ocean color missions to quantify NO_2 spatio-temporal variations with their lower spectral resolution measurements.

This paper attempts to answer the question, can NO_2 slant columns be accurately estimated with planned ocean sensors such as PACE OCI and GLIMR? If such retrievals can be achieved, they could provide improved spatial resolution of NO_2 total column amounts as compared with existing instruments, a benefit for land and ocean retrievals as well as for atmospheric science. We also explore whether the techniques developed for retrieving NO_2 from the ocean color instruments, including machine learning, can be harnessed to improve existing algorithms applied to atmospheric instruments, both in terms of quality and efficiency. State-of-the-art spectral fitting algorithms can be computationally burdensome. Algorithm efficiency is particularly important for current and future atmospheric composition instruments, including those in geostationary orbit, that have very large data volumes. Machine learning has been shown to be an efficient means of estimating NO_2 vertical columns from satellite spectra (Li et al., 2022) as well as for other applications in remote sensing and geoscience (Maxwell et al., 2018; Lary et al., 2016).

2 Data and methods

2.1 NO_2 absorption cross sections and DOAS retrievals

NO_2 absorption covers a broad range of wavelengths from the UV to the near-infrared (NIR) with a peak near 400 nm. Figure 1 shows NO_2 absorption cross sections from the UV through red wavelengths (Vandaele et al., 1998), where the blue and green curves have been convolved and resampled to approximate effective cross sections for OMI and OMPS, respectively. The red and black curves show the NO_2 cross sections convolved with boxcar functions of widths 5 and 10 nm and 2 samples per box, similar to the expected spectral resolution and sampling of OCI and GLIMR, respectively. Particularly at the OCI spectral resolution, there is still marked high frequency structure throughout the visible wavelength range.

Most NO_2 spectral fitting algorithms are based on the differential optical absorption spectroscopy (DOAS) methodology (e.g., Platt and Stutz, 2006). In a DOAS-type spectral fit, the retrieved quantity is the slant column density (SCD) of a weakly absorbing trace gas, defined as the integrated number of molecules per unit area to produce an observed amount of absorption at a particular wavelength along the total atmospheric photon path. DOAS generally works by fitting appropriately convolved absorption cross-sections (effective cross-sections) to the logarithm of sun-normalized radiance spectra for a given fitting window. A DOAS slant column retrieval for NO_2 involves fitting the high frequency structure in the NO_2 absorption cross sections generally in the range 400–497 nm (see Figure 1) while accounting for the low frequency envelope of NO_2 absorption, e.g., using a polynomial function (e.g., Richter and Burrows, 2002; Lerot et al., 2010; Richter et al., 2011; Marchenko et al., 2015; van Geffen et al., 2015, 2020). At GLIMR spectral resolution, a retrieval would likely need to make use of the broad

https://doi.org/10.5194/egusphere-2022-806
Preprint. Discussion started: 19 September 2022

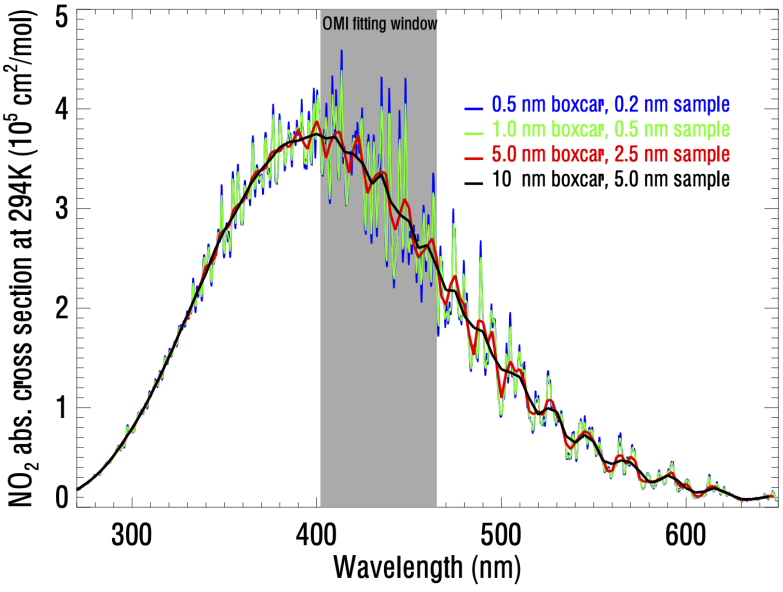

Figure 1. NO_2 cross sections from Vandaele et al. (1998) convolved with boxcar functions of different widths: Blue: similar spectral characteristics to OMI (though the OMI range limited to wavelengths <500 nm; green: similar to OMPS-NM; red: similar to OCI; black: similar to GLIMR.

continuum absorption over a wider spectral range than typical DOAS retrievals. While this type of approach has been achieved for ozone (Fleig et al., 1986) whose stratospheric column amount is typically quite large, it has not be demonstrated for gases with weaker absorption (owing in part to lower column amounts) such as NO_2.

Within any type of spectral fit, other known absorbers or pseudo-absorbers, such as rotational-Raman scattering (also known as the Ring effect), should be accounted for. In typical NO_2 fitting windows, the interfering absorbers include ozone (O_3), water vapor (H_2O), the oxygen dimer (O_2-O_2), and gloyoxal ($CHO-CHO$). The spectral imprint of the Earth's surface must also be accounted for along with other instrumental effects such as spectral alignment of the radiance spectra and proper characterization of the instrument response function.

A secondary retrieval step involves estimation of the vertical column density (VCD) of NO_2 using the SCD, sun-satellite geometry, and information about clouds, aerosols, the Earth's surface, and the NO_2 profile shape. The SCD and VCD are related through the concept of an air mass factor (AMF), i.e., VCD = SCD / AMF. Both the SCD and AMF are formally wavelength dependent, so that typical DOAS retrievals using a range of wavelengths to fit a single value SCD or compute an AMF refer to an average over the fitting window. Richter et al. (2014) have accounted for this wavelength dependence, but this type of approach is typically not used in operational algorithms. A direct VCD spectral fitting algorithm was also applied to UV wavelengths to retrieve NO_2 from the OMPS-NM (Yang et al., 2014).

https://doi.org/10.5194/egusphere-2022-806
Preprint. Discussion started: 19 September 2022

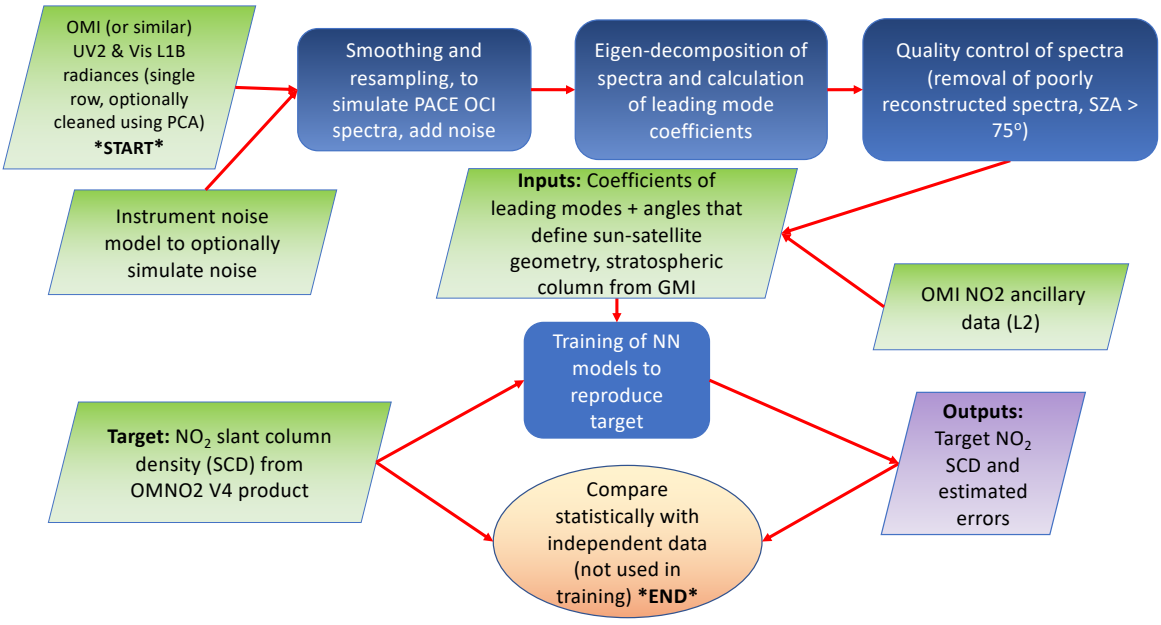

Figure 2. Data flow diagram showing simulation of radiance for a low spectral resolution hyper-spectral instrument (PACE OCI) using observations from a higher spectral resolution instrument (OMI) as well as training and evaluation of a neural network (NN) to estimate NO_2 slant column densities (SCDs).

2.2 Data flow and retrieval

Figure 2 shows a flow diagram of the data processing that we use here to train and evaluate results from a neural network (NN) that predicts NO_2 SCDs using simulated data from imagers, such as OCI and GLIMR, with lower spectral resolution as compared with spectrometers, such as OMI and TROPOMI, designed for atmospheric measurements. We simulate OCI and GLIMR observations by spectrally averaging and resampling OMI data and adding noise according to instrument specifications and measurements. A machine learning approach is then employed to estimate the OMI-derived NO_2 slant columns with simulated data from the lower spectral resolution instruments. As explained in more detail below, we focus on NO_2 SCD retrievals. The conversion of SCD to total or tropospheric VCD can be accomplished in a straight-forward and computationally efficient manner as in current algorithms and is not addressed further here. Details of the input features, target outputs, and architecture of the machine learning algorithm are provided in the following subsections.

https://doi.org/10.5194/egusphere-2022-806
Preprint. Discussion started: 19 September 2022

2.2.1 OMI radiance and NO_2 data

OMI is a push broom spectrometer that measures backscattered sunlight and solar irradiance in the spectral range 270–504 nm (Levelt et al., 2006, 2018). It employs a two dimensional (2D) charged coupled device (CCD) that provides spectral information in one dimension and spatial information in the other. This results in sixty rows of spectra in the cross track direction. Spacecraft motion provides observations along the satellite swath. Therefore, each cross track row of OMI can be considered as a distinct instrument with its own characteristics (wavelengths, response functions, calibration) and biases. The wavelengths vary slightly across the swath resulting in a so-called spectral smile. The spatial resolution is approximately 13 km in the along track direction by 24 km in the cross track direction at nadir with larger pixels towards the swath edges. The total swath width is ∼2600 km.

There are three separate detectors on OMI. We ran experiments with L1B Earthshine radiances from the OMI collection 3 for the visible (VIS) (Dobber, 2007b) and UV-2 detectors (Dobber, 2007a) that cover wavelengths from 349–504 nm and 307–383 nm, respectively. We use data from early in the mission (2005) for this study. Later in the mission, some of the rows were affected by an anomaly presumably outside the instrument that caused blockage and scattering of light into some of OMI's rows (Levelt et al., 2018) resulting in a decrease of spatial coverage.

We use the destriped SCDs (parameter name SlantColumnAmountNO2Destriped) from the collection 3 version 4.0 OMNO2 NO_2 product (Lamsal et al., 2021; Krotkov et al., 2019) as the NN training target. The NO_2 spectral fitting algorithm is based on Marchenko et al. (2015) who use an iterative approach in which the 402–465 nm range is broken up into seven smaller overlapping micro-windows. This method leads to flexible determination of wavelength-dependent shifts between radiance and irradiance spectra as well as the rotational Raman scattering or so-called Ring spectrum. The overall OMI standard NO_2 product has undergone substantial changes over the years after being evaluated in numerous studies with respect to other model-, ground-, air-, and satellite-based data sets (e.g., Lamsal et al., 2014; Choi et al., 2020, and references therein).

2.2.2 Simulated OCI and GLIMR data

We start with the OMI Level 1B (L1B) radiances. Unlike in standard OMI retrieval algorithms, we do not perform any normalization with respect to either a solar spectrum or other reference spectrum. While this normalization could be done and there may be advantages, such as for processing long time series in which instrument degradation occurs, here we elected to keep the approach as simple as possible.

The next step is to optionally reduce noise in the OMI data using a principal component analysis (PCA) approach, where spectra are reconstructed using coefficients of a limited number leading principal components (PCs) constructed from a large sample of data. Here as in standard DOAS fits, we use the natural logarithm of the radiances, but without normalization as discussed above. The goal of the noise reduction is to provide a relatively clean, though not necessarily perfect, set of spectra to simulate data for different instrument configurations. Our aim is to produce a realistic simulation of satellite observations. While we could have used simulated spectra instead of OMI data, it would be difficult to capture all of the complexities present in real satellite-observed spectra, including instrumental artifacts, and other complex interactions involving scattering and absorption in the atmosphere and surface.

https://doi.org/10.5194/egusphere-2022-806
Preprint. Discussion started: 19 September 2022

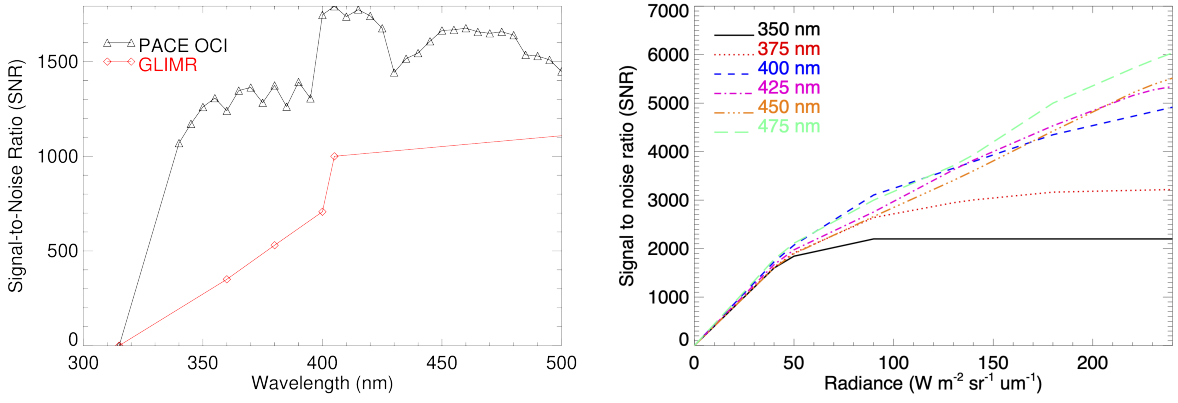

Figure 3. Instrument noise models for PACE OCI and GLIMR: a) Nominal instrument specifications of SNR for PACE and GLIMR (assumed constant with radiance level in our simulations); b) an advanced instrument noise model provided by the PACE OCI team based on preliminary measurements showing the SNR as a function of wavelength and radiance (private communication) .

The data sample used in the initial PCA starts with all observations from one day in every other month (the 15th day) in 2005 supplemented with additional days in winter when the NO_2 lifetime is long and pollution can build up in the boundary layer to give very high SCDs. The added high pollution days are 29 January through 04 February of 2005. The same data sample is used for training and evaluating the NN models as described below. Use of a large sample spanning different seasons assures that we cover a wide range of sun-satellite geometries as well as pollution, cloud, and surface conditions in the training data.

We found by trial and error that 60 PCs sufficiently reconstructs the OMI spectra in the range 349-503 nm (742 spectral samples) for the purposes of NO_2 spectral fitting, while removing spurious features that can occur for example within the south Atlantic anomaly region as described by Gorkavyi et al. (2021). In other words, beyond this number, there is not significant correlation between PCs and NO_2 absorption cross sections. The cleaned OMI L1B data are then averaged over different spectral bandpasses to simulate data from lower spectral resolution instruments. Here, we used a simple boxcar function with widths 5 and 10 nm and resampled at 2.5 and 5 nm to simulate OCI-, and GLIMR-like instruments, respectively. This produces 59 samples for the OCI-like instrument for a spectral range 355–502.5 nm. Finally, noise following a Gaussian distribution is optionally added to the simulated spectra according to instrument specifications and measurements. Figure 3a shows specified signal-to-noise ratios (SNRs) for OCI and GLIMR used here that were provided by the instrument teams, where we assume these values are independent of radiance value. Figure 3b shows an advanced SNR model for PACE OCI based on recent measurements that is expected to be closer to the actual instrument performance, where the SNR varies with radiance. Typical radiance distributions for different wavelengths are shown in Appendix A.

https://doi.org/10.5194/egusphere-2022-806
Preprint. Discussion started: 19 September 2022

2.2.3 Machine Learning Architecture

The machine learning algorithm was constructed within the Interactive Data Language (IDL) software package. It consists of a three layer feed-forward artificial NN with two hidden layers and 1.3N nodes in each layer, where N is the number of inputs (Schmidhuber, 2015). Details regarding the inputs are given below. The output layer has OMI NO_2 SCD as a single node. We use a soft-sign activation function for the first layer, a logistic (sigmoid) for the second layer, and a bent identity for the third layer. An adaptive moment estimation optimizer minimizes the error function with a learning rate of 0.1. We scale all inputs and outputs such that means are zero and standard deviations are equal to unity.

2.2.4 NN inputs

We perform a PCA (or eigen-decomposition) of the simulated spectra using the same data sample as described above for the noise reduction. The coefficients of a leading number of PCs are used as inputs to the NN. We find that the NN training converges faster when coefficients of the PCs are used rather than the measured radiances themselves, even when coefficients of all modes are used as inputs. The PCA concentrates the spectral features corresponding to information about the atmosphere and surface in the leading modes while projecting the random instrument noise onto the trailing modes. This may make it easier for the NN to reject those coefficients with little information content pertaining to the target. We found, by trial and error, that maintaining a number of PCs equal to half the number of spectral elements was sufficient to capture the spectral information associated with NO_2 while providing some noise reduction.

We then perform quality control on the spectra. We remove all data with slant columns less than zero or greater than 1×10^{17} molec cm^{-2}. We also remove any pixels where the solar zenith angle (SZA) is greater than 75°. Finally, we check that the quality flag on the OMI SCD data indicates a good fit.

The inputs to the NN are then the coefficients of the leading PCs and other optional parameters that may aid the NN in trying to match the target OMI NO_2 SCD output variable. An important consideration for selection of input parameters is that we are training a NN to estimate SCDs produced by a DOAS-like algorithm that used a more narrow fitting window weighted towards the blue spectral region as noted in Figure 1. SCDs, because they depend upon the atmospheric photon path, are by definition wavelength dependent. UV wavelengths have less sensitivity to lower tropospheric NO_2 than blue wavelengths owing to the effects of Rayleigh scattering that increase towards the UV and generally reduce the amount of light reflected from the surface (Richter et al., 2014).

The NN training is performed separately for each OMI CCD detector row, because each row has unique spectral characteristics. While it is possible to perform NN training on all rows at once, since the data are spectrally averaged to a uniform wavelength grid as in Fasnacht et al. (2022), we find that slightly better performance is achieved by training on each row individually.

We tested several parameters that can help to determine how much of the OMI-derived SCD originates from the lower troposphere where UV wavelengths have less sensitivity. These include the cosine of the solar and view zenith angles, cosine of the scattering angle, the stratospheric NO_2 column from the Global Modeling Initiative (GMI) chemical transport model, the

https://doi.org/10.5194/egusphere-2022-806
Preprint. Discussion started: 19 September 2022

geometry-dependent Lambertian-equivalent reflectivity (GLER) of the surface (Vasilkov et al., 2017, 2018; Qin et al., 2019; Fasnacht et al., 2019), surface pressure, and the effective scene pressure that is related to both the cloud pressure and optical thickness. Over ocean, the GLER accounts for the anisotropy of solar reflection from the ocean surface and backscatter from the bulk of ocean water and over land accounts for the bidirectionality of scattered sunlight from shadowing in vegetation. We also tried to use the stratospheric column provided by the Global Modeling Initiative (GMI) model multiplied by the stratospheric air mass factor, or in other words the expected stratospheric SCD based on the model estimate.

The parameters that were ultimately selected as input features are shown in Fig. 2. We find that the combination of stratospheric column NO_2 and the cosines of solar zenith and scattering angles slightly improve the estimates of the target OMI NO_2 SCDs as discussed in more detail below. The cosine of the view zenith angle is nearly constant for a given row and does not provide significant improvement. The other inputs tested similarly did not substantially improve the fitting. The spectra themselves contain information about these variables, although the training of the NN may require more iterations if these variables are not included as predictors. For example, information about the cloud optical thickness and underlying surface is present in the radiances and can be disentangled using machine learning (Joiner et al., 2022; Fasnacht et al., 2022). Information about cloud pressure is contained within the oxygen dimer absorption band near 477 nm (Acarreta et al., 2004) as well as from the filling-in of solar Fraunhofer lines by rotational-Raman scattering (e.g., Joiner and Bhartia, 1995). We take a minimalist approach here with respect to the predictors and below only include stratospheric column amount and the cosines of solar zenith and scattering angles as features in the results shown below.

2.2.5 NN outputs

We also tested a variety of different target outputs. We tested both NO_2 SCD and the natural logarithm of the NO_2 SCD as target outputs. We find that slightly better results are obtained using the natural logarithm of the NO_2 SCD. This may be expected because this variable has a more normal distribution. BoxCox transformations (Box and Cox, 1964) may produce slightly better results yet, but will depend upon the sample used. As the distributions of NO_2 have undergone changes with time, particularly in polluted regions, results obtained by training on a single distribution may not be optimal for a given time period.

We also tried training directly on the total VCD. More iterations for training may be needed owing to complex relationships with atmospheric constituents and the Earth's surface that impact the photon pathlength and that are needed to estimate the VCD including dependencies on clouds, aerosol, and the surface bi-directionality. Without detailed knowledge of the NO_2 profile (we used only estimates of the stratospheric and tropospheric columns from the GMI), we did not obtain a satisfactory result and for simplicity focus on SCD exclusively as the target parameter below. The conversion from SCD to VCD can be achieved efficiently using existing algorithms.

2.2.6 NN training and evaluation

For the training, we used every other data point from the sample described above, providing more than 100,000 samples for each row. We then compare statistical results including variance explained (r^2), bias defined as the mean of SCD_{true} - SCD_{est}, where

https://doi.org/10.5194/egusphere-2022-806
Preprint. Discussion started: 19 September 2022

SCD_{true} and SCD_{est} are the true (from OMNO2) and estimated NO_2 SCDs, respectively, and root-mean-squared difference (RMSD = $\sqrt{(\sum_{n=1}^{N}[SCD_{n,true} - SCD_{n,est}]^2)/N}$) based on independent samples (i.e., not used in the training set). We did not find evidence of overtraining. We also use a completely independent day (28 January 2005) for visual evaluation below.

2.3 Addressing instrumental noise in the training process

There are several possible ways of dealing with the effects of instrumental noise in the training and application of NNs. One method is to train a NN using noiseless data, then apply the trained network to noisy data. Another method is to train a NN using noisy data. The latter approach is likely to provide the best result as the NN learns how to properly weight the different wavelengths based on a large sample that provides information about the wavelength dependence of the SNR. The former approach may work well if the SNR is relatively constant with wavelength. Another advantage to the former approach is that only one trained network is needed for either simulations or application to real data where the inputs could have a variety of different SNRs.

To mitigate the impact of instrumental random noise, one may either spatially average the noisy SCD retrievals or spectrally average radiance observations from adjacent fields-of-view (FoV) and use the coefficients computed with averaged spectra as inputs to the trained NN. If there are spatially dependent biases in the SCD results obtained with noisy data, these biases will not be eliminated by averaging together noisy retrievals. Therefore, it may be more advantageous to average spectra together and present the averaged data as inputs to a NN. The disadvantage to this approach, as described above, is that for optimal results, one may need to train a separate NN for each SNR scenario. We tested all of these approaches and found that the best results were obtained by averaging spectra together and training separate NNs for each SNR scenario. In practice, spatially averaging of pixels would be employed to increase the SNR, thus degrading the spatial resolution of the resulting retrievals.

3 Results

3.1 Results with simulated PACE OCI spectra

We tested approaches initially using spectra from OMI UV-2 and Vis channels with a range of 325–502.5 nm. Here, we concatenated spectra from the two channels using UV-2 for wavelengths < 355 nm and Vis for the remaining range. There was only a slight discontinuity in the joined spectra at the overlap wavelength. However, we found that use of the UV-2 wavelengths did not significantly improve results as compared with those using the Vis channel alone. Therefore, all results shown below are obtained using a range or subset of the range 355-502.5 nm obtained with the OMI Vis channel only. We note that there is a slight spatial mismatch between OMI UV-2 and Vis channels that may have contributed to the overall lack of improvement using UV-2 wavelengths. In addition, there is limited high frequency spectral structure in the convolved NO_2 absorption cross sections in the UV-2 range. When PACE OCI data become available, we encourage testing again using all available wavelengths including those with wavelengths > 502.5 nm that are not available from OMI.

https://doi.org/10.5194/egusphere-2022-806
Preprint. Discussion started: 19 September 2022

Table 1. Statistical comparison of retrievals for row 1 simulated with the advanced SNR model (Fig 3b), using 17390 independent data points on 28 January 2005 (day not used in training) for simulated PACE OCI NO_2 SCD. "All" refers to the use of all spectral data from the fitting window along with cosines of the solar zenith and relative azimuth angles (angs.) as well as the stratospheric column (strat. col.); statistics include the root mean squared difference (RMSD), bias, and variance explained (r^2) of the SCD. Bias and RMSD are given in units of 10^{15} molec cm^{-2}.

NN inputs	fitting window (nm)	r^2	bias	RMSD
all	355-500	0.943	-0.133	0.993
no angs.	355-500	0.938	-0.156	1.040
no strat. col.	355-500	0.925	0.023	1.159
no angs., no strat. col.	355-500	0.918	-0.183	1.198
all	400-470	0.934	-0.198	1.075
all	400-500	0.938	-0.205	1.047
no strat. col.	400-500	0.926	-0.294	1.201
no angs., no strat. col.	400-500	0.918	-0.172	1.192

Table 1 shows the results of testing with different wavelength ranges and inputs on a single OMI row (row 1, zero based) and with the advanced SNR model (Fig 3b). We find that using more restricted wavelength ranges leads to only a small degradation in the results as compared with the full range of 355–500 nm. For example, the range 400-500 nm slightly degrades the results, while further reducing the range to 400-470 nm leads to a bit more degradation. This is consistent with the full spectral resolution results of Li et al. (2022) who found an optional retrieval window of 390–495 nm for estimating NO_2 vertical columns. Our results indicate that most of the information for NO_2 at OCI spectral resolution is provided by the high frequency structure of the radiances produced by NO_2 absorption within the fitting window currently used in the OMNO2 product. Little additional information is provided by UV wavelengths that define the more broad NO_2 absorption feature. In addition, we show that removing the geometrical information (cosines of the solar zenith and relative azimuth angles) results in only a small degradation. The use of an estimate of the stratospheric column NO_2 does appear to aid the estimation of the NO_2 SCD, even with reduced fitting windows.

Table 2 shows results of the trained NN applied to data from all rows on 28 January 2005, a day not used in training. Simulations without noise produced quite reasonable results, capturing about 95% of the variability with little overall bias. Here, we report statistics for SCDs normalized by the stratospheric AMF (essentially assumes that all NO_2 is in the stratosphere) to give a rough estimate of the VCD. Results degrade noticeably when the nominal noise (using SNR from Fig. 3a) is applied to the simulated spectra; variability captured drops to about 90.5% and the RMSD increases from 0.27 to 0.38 $\times 10^{15}$ molec cm^{-2}. Results are improved with the advanced SNR model from Fig. 3b that shows better instrument performance (variability captured increases to 91.6%). The advanced SNR model provides results that are comparable to what would be achieved by averaging together 4 pixels that have performance corresponding to the nominal noise model (variability captured in the latter

https://doi.org/10.5194/egusphere-2022-806
Preprint. Discussion started: 19 September 2022

Table 2. Statistical comparison of 1,113,061 points on 28 January 2005 (day not used in training) for simulated PACE OCI slant column density normalized by stratospheric air mass factor with the nominal (nom.) SNR model (Fig. 3a) and the advanced (adv.) SNR model (Fig. 3b). Statistics include the root mean squared difference (RMSD), bias, and variance explained (r^2) of the normalized SCD (normalized by the stratospheric air mass factor). Bias and RMSD are given in units of 10^{15} molec cm^{-2}.

instr.	noise	r^2	bias	RMSD	area (km^2)
OCI no noise	N	0.950	0.023	0.273	1
OCI nom. SNR	Y	0.905	0.049	0.377	1
OCI adv. SNR	Y	0.916	-0.038	0.353	1
OCI nom. SNR $\times$ 2	Y	0.921	0.038	0.342	4
OCI nom. SNR $\times$ 4	Y	0.934	0.030	0.313	16
OCI nom. SNR $\times$ 4, rows 10-50	Y	0.923	-0.033	0.337	16
OCI nom. SNR $\times$ 4, rows 0-10, 50-59	Y	0.955	-0.023	0.258	16

scenario is 92.1%). More than half of the degradation that results from adding the nominal noise is recovered when the nominal SNR is increased by a factor of 4. Such an increase in SNR could be achieved by averaging together spectral from a 4×4 array of OCI pixels to give an area of approximately 16 km^2. We also looked at how the performance varies across the OMI swath. We found better performance at the OMI swath edges where the SCD values are largest leading to deeper absorption features (last two lines of Table 2; swath edges are the rows with both the highest and lowest values). Even when normalized by the SCD, the performance enhancement at the swath edges remains.

The results for GLIMR, even with no noise, were not satisfactory (r^2 around 0.86 and substantially worse with added noise) and are not shown. One reason for this result is the lack of spectral structure in the NO_2 effective cross sections at GLIMR resolution. Another factor is that there are many fewer available spectral samples for GLIMR, and therefore the impact of the instrumental noise is substantial.

Figure 4 shows results obtained with data from 28 January 2005 using the PACE OCI SNR $\times$ 2 scenario. Here, we show the unnormalized SCD, and statistics therefore differ from the normalized SCD results shown in Table 2. The bulk of the SCDs are in the approximate range of $4 - 10 \times 10^{15}$ molec cm^{-2}. Figure 4b shows that apart from one row, there is little evidence of striping (systematic row dependent errors) in the NN results. Note that there was no attempt to destripe the SCDs on this day of independent data as is done on a daily basis in the OMNO2 data used to train the NN. Striping can occur on an orbital or daily basis which is why OMNO2 initial SCDs undergo a destriping process. Figure 4c shows that there are some systematic differences between OMNO2 and the NN SCDs as a function of latitude. For example, there is a low bias in the NN-derived SCDs at low southern latitudes (over Antarctica), a high bias at tropical latitudes, and some low biases at high northern latitudes that tend to occur for higher values of SCD (see Fig. 4a,d), likely over polluted regions. Performance may vary as a function of surface reflectance and cloud conditions.

Figure 5 shows an example of how the NO_2 SCD errors may be spatially correlated. Because we use OMI data as the “truth" or target for training, simulated PACE OCI results are shown at the OMI spatial resolution rather than at the OCI resolution.

https://doi.org/10.5194/egusphere-2022-806
Preprint. Discussion started: 19 September 2022

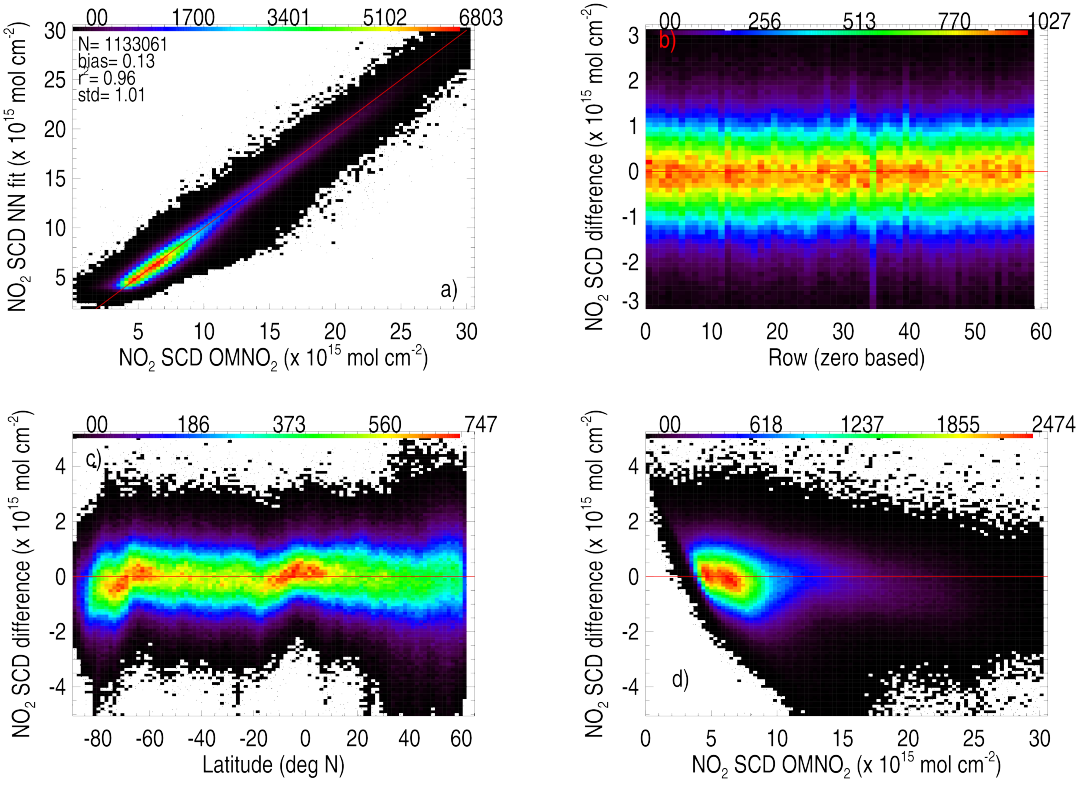

Figure 4. Global data from 28 February 2005 from a training using where each point represents the result that would be obtained using the nominal OCI SNR from Fig. 3a multiplied by 2; a) Density distribution (numbers along the top) of NO_2 target OMNO2 SCD (all results here are not normalized with respect to an air mass factor) versus those from the NN training with statistics include standard deviation of the difference (std), fraction of variance explained (r^2), and mean of difference between NN and target (bias); b-d) density distribution of the NO_2 SCD difference (NN SCD - OMNO2 SCD) as a function of OMI row number, latitude, and NO_2 SCD, respectively.

The reader must imagine that real OCI results can be obtained at a spatial resolution as high as 1 km × 1 km, rather than at the OMI resolution (12 km × 24 km at nadir) shown here. Judd et al. (2020) provide examples of fine resolution NO_2 over an urban area as measured from an aircraft instrument.

Here, we display retrieved SCDs based on simulations at various SNR levels on 28 January 2005, a day with high pollution over northeast and midwest portions of the United States. Figure 5a shows the original OMNO2 SCDs normalized by the stratospheric AMF to provide values similar to the total VCD. These are considered as the true values used for comparisons with those from simulated OCI retrievals. Figure 5b shows the estimated fraction of radiance coming from cloudy portions of a pixel (cloud radiance fraction). In areas that have cloud radiance fractions approaching unity, most of the observed NO_2 SCD would result from NO_2 in the stratosphere or upper troposphere owing to clouds that screen the polluted atmosphere below

https://doi.org/10.5194/egusphere-2022-806
Preprint. Discussion started: 19 September 2022

them from satellite view. Note that pixels with snow cover that is not reported in the input snow/ice dataset will be reported as cloud cover.

Results obtained using the simulated PACE OCI spectra with no noise added (Fig. 5c,d) show very little regional bias, with the largest errors occurring over highly polluted areas. Low biases over polluted regions may be expected as wavelengths in the UV, that OCI retrieval relies upon, have less sensitivity to NO_2 in the boundary layer where NO_2 can accumulate in high pollution conditions. This "no noise" case represents the best result (upper limit) that can be expected based on the OCI sampling and spectral resolution.

The effects of the expected PACE OCI nominal instrument noise, shown in Figure 5e and f, degrade the results with noticeably higher noise in NO_2 SCDs over the relatively clean oceanic regions and a generally low bias over highly polluted areas. Figure 6a-d shows results of simulations using the nominal OCI SNR multiplied by 2 or 4. Figure 6e-f displays results using the advanced OCI SNR model (Figure 3b). Results obtained with this model are similar to those of nominal OCI SNR model multiplied by 2. This is not surprising as the advanced SNR model values are approximately a factor of 2 higher than the nominal noise model at typical radiance values and for wavelengths longer than about 375 nm. The effect of increasing the SNR reduces regional biases in high pollution areas.

3.2 Practical implementation issues

We next address how our approach can be practically implemented with a high spatial resolution, low spectral resolution hyperspectral sensor such as PACE OCI that we will refer to as the imager and an existing moderate spectral resolution spectrometer such as OMI or TROPOMI that we will refer to as the spectrometer. The desired retrieved quantity for atmospheric correction in ocean color algorithms is not the NO_2 SCD, but rather the VCD. Once a NN is trained to produce NO_2 SCD from input spectra, the SCDs may be converted to VCD using a computed AMF that will be a function of the sun-satellite geometry, surface and cloud conditions, and NO_2 profile shape as described above and shown in Figures 7-8. This is typically accomplished with lookup tables and model-generated NO_2 profiles. With the NO_2 VCD, the spectral transmittance due to NO_2 can then be computed with a radiative transfer model that will be a function of wavelength, the surface albedo, and other absorbers and scatters in the atmosphere. This last step may be performed with either table lookup or machine learning.

To use NO_2 SCDs from TROPOMI or similar spectrometer for training of a NN with a collocated spectra from a higher spatial resolution hyperspectral instrument, such as OCI, as inputs for the purpose of estimating SCDs from the imager, it is necessary to use radiative transfer to transform the SCDs from the spectrometer to the appropriate sun-satellite geometry of the imager as shown in Figure 7; the overlap between these two instruments on different satellites will not typically occur for the same sun-satellite geometries. One approach to prepare a training data set would be to use the total VCD retrievals from the spectrometer (e.g., TROPOMI) to derive an estimated SCD for the imager (e.g., OCI) at its geometry. One can simply apply computed AMFs at the appropriate geometries. This can be written as

$$\mathrm{SCD}_{\mathrm{imager}} = \mathrm{SCD}_{\mathrm{spectrometer}}/\mathrm{AMF}_{\mathrm{spectrometer}} \times \mathrm{AMF}_{\mathrm{imager}} = \mathrm{VCD}_{\mathrm{spectrometer}} \times \mathrm{AMF}_{\mathrm{imager}}, \quad (1)$$

https://doi.org/10.5194/egusphere-2022-806
Preprint. Discussion started: 19 September 2022

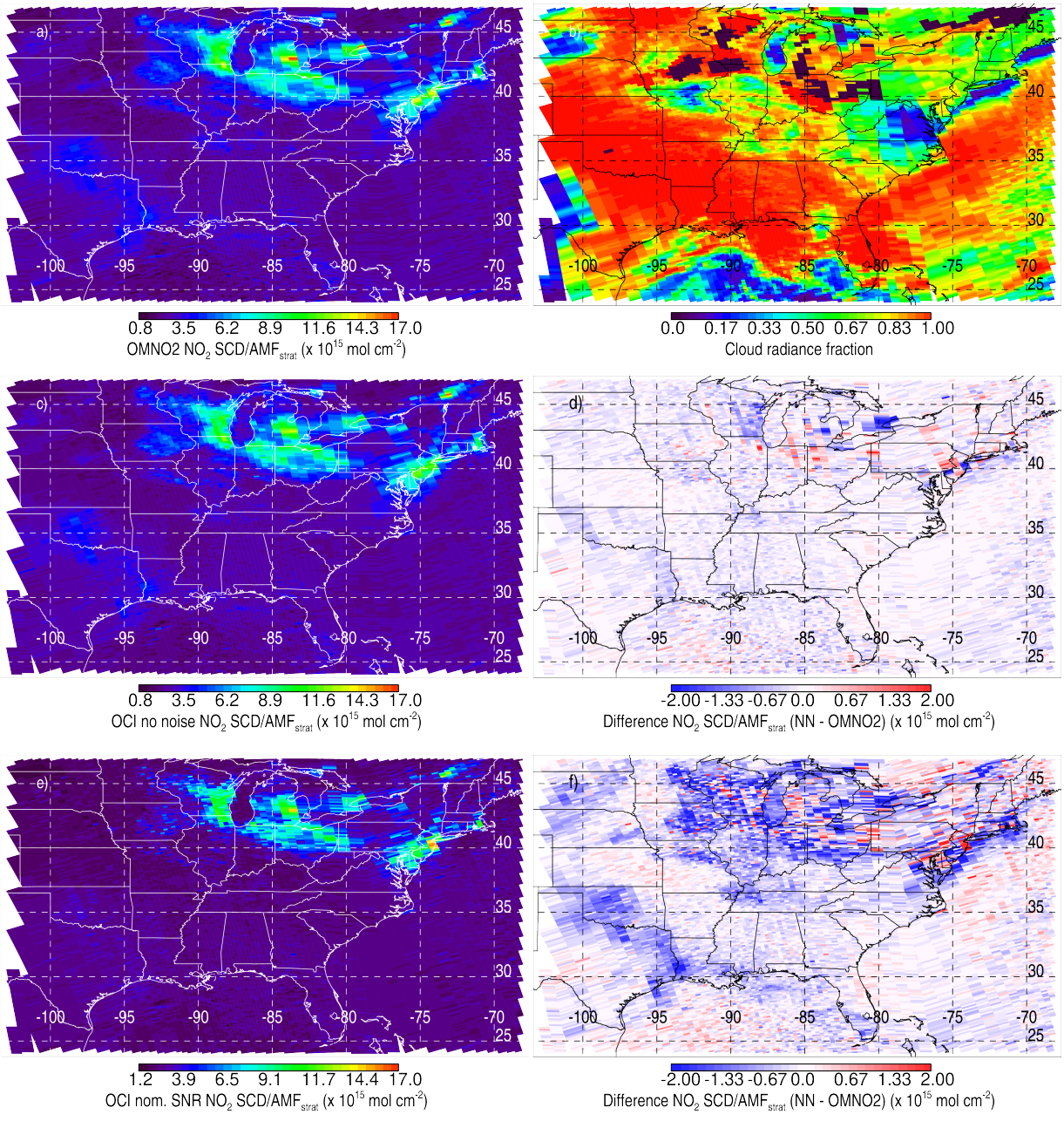

Figure 5. Data from 28 January 2005 (day not used in fitting): a) NO_2 SCDs normalized by the stratospheric air mass factor (normalized SCD) from the OMI OMNO2 algorithm; b) Cloud radiance fraction for the NO_2 fitting window from OMNO2; c), e): Normalized SCDs from the NN algorithm evaluated at each OMI pixel using OCI spectral characteristics with no noise and the nominal SNR, respectively ; d), f): corresponding differences with respect to OMNO2 normalized SCDs.

https://doi.org/10.5194/egusphere-2022-806
Preprint. Discussion started: 19 September 2022

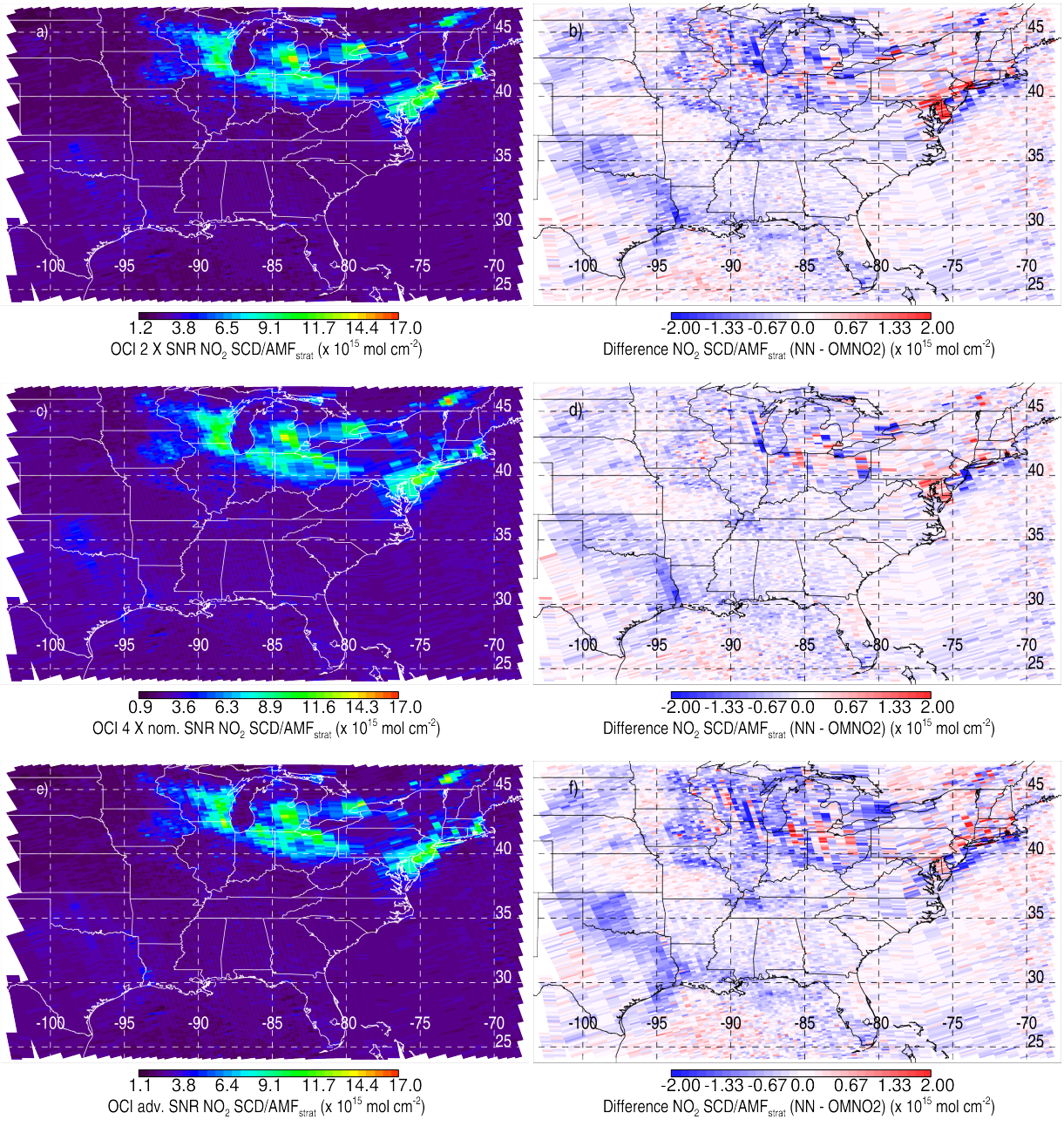

Figure 6. Data from 28 January 2005 (day not used in fitting): a), c), e): NO_2 SCDs normalized by the stratospheric air mass factor (normalized SCD) from the OMI OMNO2 algorithm, from the NN algorithm evaluated at each OMI pixel using OCI spectral characteristics with 2× nominal SNR, 4× nominal SNR, and with the advanced (adv.) SNR model, respectively; b), d), f): corresponding differences with respect to OMNO2 normalized SCDs shown in Fig. 5a.

https://doi.org/10.5194/egusphere-2022-806
Preprint. Discussion started: 19 September 2022

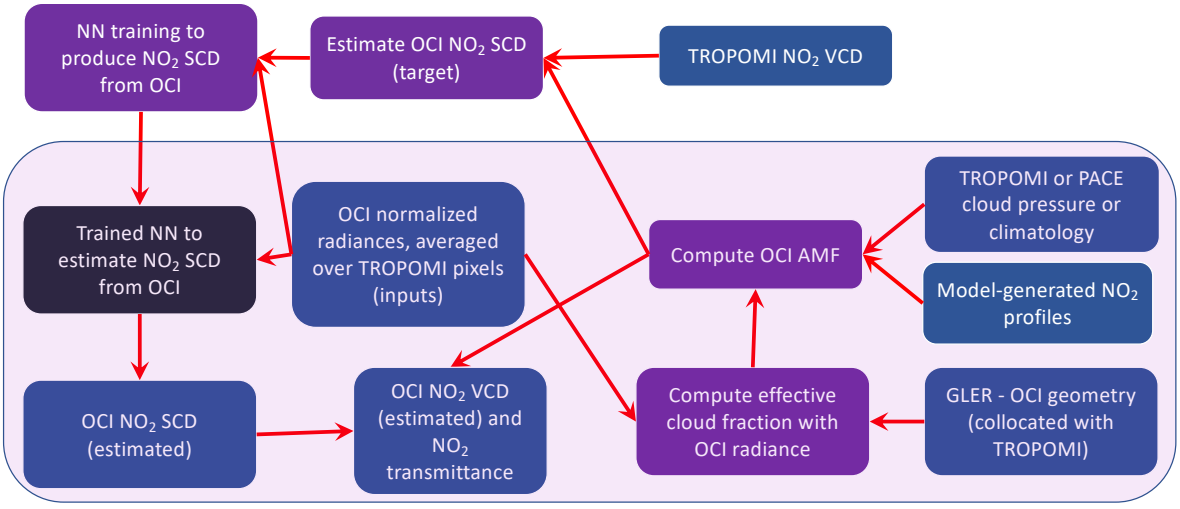

Figure 7. Flow diagram showing processes and data needed to estimate the NO_2 VCD using TROPOMI data collocated to OCI. Data sets are indicated by blue boxes, dynamic processes with purple, and a static process in black. Components needed to compute the VCD once the neural NN training process is complete are shown within the light purple overlay.

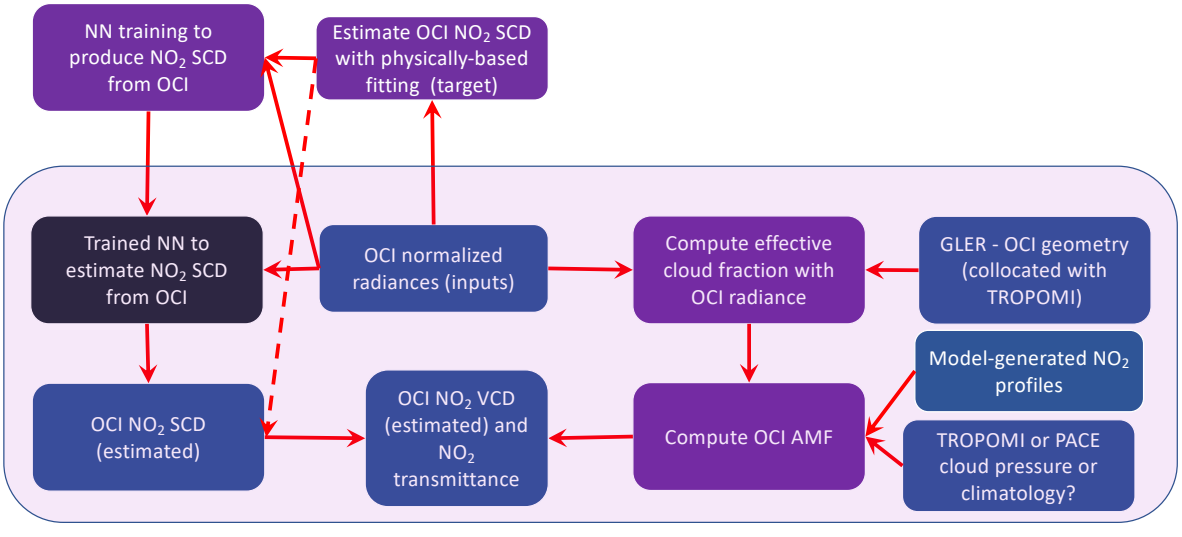

Figure 8. Similar to Figure 7 but showing processes to estimate NO_2 VCD using only OCI data. The dashed line shows an alternative flow that does not require training a neural network.

where AMF_{imager} is the AMF computed using the same inputs as for the spectrometer (e.g., cloud radiance fraction, NO_2 profile shape, etc.) but using the appropriate sun-satellite geometry, including its impact on surface bi-directional reflectance (currently accomplished using the GLER framework), for the imager observation. This kind of approach could be made to work

https://doi.org/10.5194/egusphere-2022-806
Preprint. Discussion started: 19 September 2022

relatively quickly with mature and well validated VCDs from a spectrometer without need to understand or make adjustments for instrumental artifacts in the imager.

Another practical consideration is that the imager spatial resolution will be higher than that of the spectrometer. One way to prepare a collocated training set would involve averaging the spectra from the imager to match the footprints of the spectrometer. This averaging will effectively change the SNR of the imager data as compared with that at its native spatial resolution. The resulting training will therefore not be optimized for application at the native resolution. If the trained network is then applied at the native resolution of the imager, the results will have to be carefully validated and checked. Another possible approach would be to spatially interpolate the spectrometer data to the locations of the imager or to perhaps use a high resolution model to downscale the spectrometer data to the resolution of the imager. Addressing these details is beyond the scope of the present work and will be dealt with in future studies.

One advantage of using collocated data from a spectrometer is that a fitting algorithm would not have to be developed and tested for the imager. We have found that developing and validating such algorithm can require significant human resources. However, our results suggest that it is possible to develop a fitting algorithm for the imager by exploiting the high frequency structure of NO_2 absorption. Such an approach, not requiring collocated data from another instrument, can be considered as an alternative approach. Spectral fitting algorithms can be computationally intensive and it may still be desirable to use machine learning to speed up the processing of dense imager data as shown in Figure 8. For example, Li et al. (2022) found that a NN implementation for NO_2 vertical columns using TROPOMI spectra was about 12 times faster than a full implementation using a priori profiles from a high spatial resolution chemistry-transport model.

3.3 Use of a neural network for exploiting additional spectral information in NO_2 slant column retrievals

We next explore the use of UV (wavelengths down to 355 nm) and longer blue wavelengths (up to 500 nm) in addition to those currently used in the OMNO2 spectral fit for the purpose of noise reduction in current algorithms. In addition, a NN implementation may have the benefit of significantly reducing computation time of the spectral fitting algorithm. The large tested fitting window has typically not been used in NO_2 in an operational setting as there are significant spectral interferences, e.g., from large Raman scattering in the Ca H and K lines in the 390–400 nm range, O_2-O_2 absorption at 360 nm, 380 nm, and 477 nm, as well as O_3 absorption for wavelengths $>$ 460 nm. Machine learning with coefficients of PCs as inputs may be adept at filtering out these interferences.

We trained a NN using OMI spectra convolved with a 1 nm boxcar function and sampled at 0.5 nm so as to produce a slightly spectrally degraded version of the original radiances. Our goal here is to not perfectly reproduce the OMNO2 target SCDs, but rather to test whether the additional wavelengths within a spectral fit improve performance in terms of reducing spatially random noise. For the following experiment with real OMI data, our assumption over a generally clean environment (Pacific ocean) is that variability in NO_2 SCD, due to clouds for example, is relatively small. In this region, the majority of the NO_2 column resides in the stratosphere and upper troposphere, where UV wavelengths have good sensitivity. For this experiment, to optimize results for a given day, we train on a smaller set of days closer to that day. We use the same training approach as above except that we use data from 29 January through 02 February 2005 for training and choose one of every three pixels for

https://doi.org/10.5194/egusphere-2022-806
Preprint. Discussion started: 19 September 2022

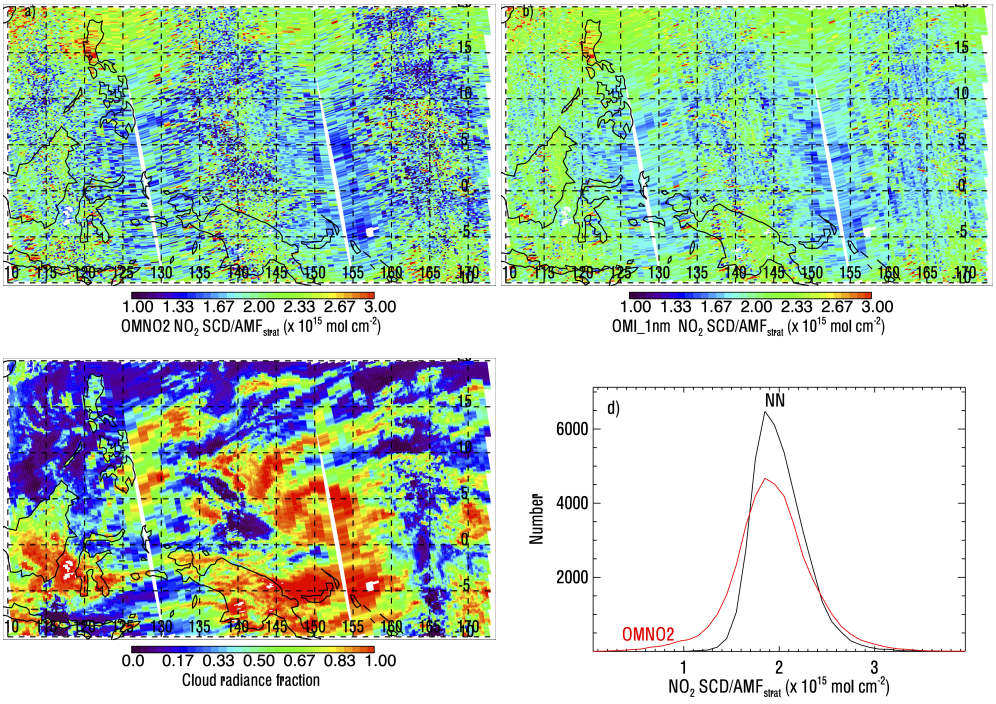

Figure 9. Normalized NO_2 SCDs from 28 January 2005 over the tropical Pacific region from a) OMNO2 and b) NN using 1 nm bandpass sampled every 0.5 nm; c) cloud radiance fraction; d) histograms of the normalized SCDs corresponding to the area shown in a).

the training sample. As above, the NN inputs are a subset of PCA coefficients, and we evaluate using data from an independent day (28 January 2005).

In Figure 9a,b, there appears to be a noticeable reduction in random noise over this clean region in the NN results obtained using the additional spectral coverage in the range 355–500 nm. The noise reduction is particularly apparent over highly cloudy regions (see Fig. 9c) where the atmosphere below the clouds is shielded from satellite view and the majority of the observed SCD is in the stratosphere. Figure 9d shows a histogram of the retrieved normalized SCDs from the target OMNO2 and the trained NN that uses additional wavelengths. OMNO2 has more pixels in the tails in the distribution, particularly at the low end. Negative SCDs are sometimes reported in the OMNO2 data set. These are retained for statistical purposes although they are physically unrealistic. The trained NN substantially reduces these low values and also reduces the number of pixels at the high SCD tail of the distribution. This experiment suggests that it is possible to utilize additional spectral range for the estimation of NO_2 SCDs. Machine learning appears to be quite effective in isolating information about NO_2 in the spectra while rejecting interfering spectral features. We similarly trained a NN to perform NO_2 SCD retrievals with the same wavelength range but at two different spectral resolutions: 1) the original OMI resolution and sampling and 2) OCI spectral resolution and sampling (no additional noise added). Similar results, showing SCD noise reduction for the clean Pacific region, are obtained using simulated data at both spectral resolutions.

https://doi.org/10.5194/egusphere-2022-806
Preprint. Discussion started: 19 September 2022

4 Conclusions

We have simulated data from the hyper-spectral imagers PACE OCI and GLIMR using OMI to demonstrate that it is possible to retrieve NO_2 SCD with reasonable accuracy and precision using lower spectral resolution data from the PACE OCI. Instrumental noise significantly impacts the results as does the spectral resolution and sampling. Better results are obtained in cases of NO_2 pollution contained in the boundary layer when the spectral resolution is high enough (of the order of 5 nm or better) to capture some of the higher frequency spectral structures in the blue part of the NO_2 absorption spectrum. Similar to TROPOMI, the longest OMI wavelength is at about 500 nm; OCI spectral coverage will continue to longer wavelengths in the green and yellow parts of the spectrum where NO_2 has additional absorption features. The added spectral range may improve results over those shown here, although the magnitude of improvement is not expected to be dramatic. Averaging spectra from several adjacent OCI pixels together will improve performance of NO_2 retrievals from PACE OCI that may be used for atmospheric correction in ocean color retrievals.

There are other potential applications for PACE OCI NO_2 retrievals. Currently, NO_2 tropospheric column density retrievals from instruments such as OMI and TROPOMI are averaged over various time periods to reduce the impacts of retrieval noise and meteorology (e.g., Lamsal et al., 2015; Duncan et al., 2016). Similar averaging of PACE OCI spectra over time, e.g., of the order of a month or more, may produce good quality data at higher spatial resolution than is available from TROPOMI. This higher spatial resolution data could then be used to downscale TROPOMI and historical OMI retrievals or could be used for emissions estimates, for example using recently developed methods for high resolution data (Liu et al., 2022). Use of high resolution averages is also useful for studies involving health impacts, including investigations involving environmental inequities (e.g., Goldberg et al., 2021; Kerr et al., 2021; Cooper et al., 2022).

We also showed that our machine learning based retrieval approach for OCI can be used to reduce noise in retrieved NO_2 SCDs in unpolluted situations for spectrometers such as OMI and TROPOMI. This result is enabled by the use of a wider spectral range and the broad continuum of NO_2 absorption. An additional advantage of using machine learning for noise reduction in spectral fitting is that once trained, an applied neural network is an extremely efficient algorithm. The current OMNO2 spectral fit is the most computationally intensive portion of the OMNO2 NO_2 tropospheric column retrieval algorithm. This may be an important consideration with the new generation of sensors in geostationary orbit with very large data volumes (Zoogman et al., 2017). These include the Korean Geostationary Environment Monitoring Spectrometer (GEMS), NASA Tropospheric emissions: Monitoring of pollution (TEMPO), and Copernicus Sentinel 4. Training could be applied intermittently throughout the data record to ensure that time-varying instrumental artifacts are accounted for. We stress that a high quality physically-based fitting algorithm is a necessary part of any machine learning approach as it produces the retrievals needed as the training target. Our machine learning approach is not meant to replace these algorithms, but rather to enhance and speed them up.

Data availability. OMI level 1B and level 2 NO_2 products used in this study are available from the GES-DISC at https://disc.gsfc.nasa.gov as cited in the manuscript.

https://doi.org/10.5194/egusphere-2022-806
Preprint. Discussion started: 19 September 2022

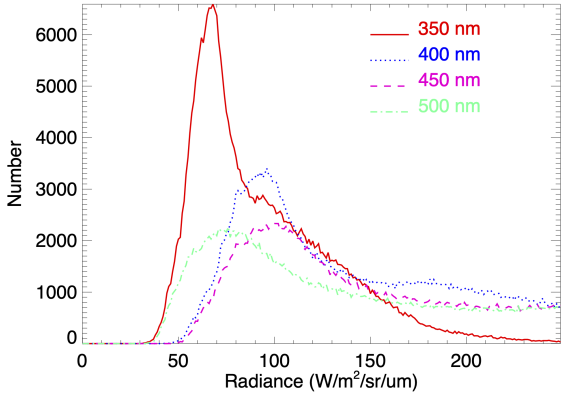

Figure A1. Histograms of radiance at different wavelengths from OMI row 1 (zero based) data taken over a range of orbits as described above.

Appendix A: Typical radiance distributions

Figure A1 shows typical radiance distributions for OMI row 1 taken over the same orbits as used for the neural network training as described above. The radiance distribution depends upon how the incoming solar irradiance is modified by gaseous and particle scattering and absorption in the atmosphere as well as surface reflectance properties.

Author contributions. JJ was responsible for the design of the methodology, investigation, including software, visualization, calculations, and formal analysis, and wrote the first draft of the article. JJ, AV, and NK provided overall supervision of the project. NK and JJ contributed to funding acquisition. LL, NK, ZF, CL, and SM provided guidance on the use of OMI products. All authors contributed to article revision, read, and approved the submitted version.

Competing interests. The authors declare that they have no conflict of interests.

Acknowledgements. The authors thank the international OMI team that produced and distributed the OMI data sets used here. They also thank the PACE OCI and GLIMR teams, particularly Antonio Mannino, Bryan Franz, Shihyan Lee, Amir Ibrahim, Andrew Sayer, Brian Cairns, and Gerhard Meister who provided the signal-to-noise (SNR) estimates used here and assistance in simulating PACE OCI and GLIMR data. Finally, the lead author thanks Arlindo da Silva for enlightening conversations. This work was supported by NASA through the PACE and Aura science team programs.

https://doi.org/10.5194/egusphere-2022-806
Preprint. Discussion started: 19 September 2022

References

Acarreta, J. R., De Haan, J. F., and Stammes, P.: Cloud pressure retrieval using the O_2-O_2 absorption band at 477 nm, Journal of Geophysical Research: Atmospheres, 109, https://doi.org/https://doi.org/10.1029/2003JD003915, 2004.

Ahmad, Z., McClain, C. R., Herman, J. R., Franz, B. A., Kwiatkowska, E. J., Robinson, W. D., Bucsela, E. J., and Tzortziou, M.: Atmospheric correction for NO_2 absorption in retrieving water-leaving reflectances from the SeaWiFS and MODIS measurements, Applied Optics, 46, 6504–6512, https://doi.org/10.1364/AO.46.006504, 2007.

Bak, J., Liu, X., Kim, J.-H., Haffner, D. P., Chance, K., Yang, K., and Sun, K.: Characterization and correction of OMPS nadir mapper measurements for ozone profile retrievals, Atmospheric Measurement Techniques, 10, 4373–4388, https://doi.org/10.5194/amt-10-4373-2017, 2017.

Boersma, K. F., Eskes, H. J., Veefkind, J. P., Brinksma, E. J., van der A, R. J., Sneep, M., van den Oord, G. H. J., Levelt, P. F., Stammes, P., Gleason, J. F., and Bucsela, E. J.: Near-real time retrieval of tropospheric NO_2 from OMI, Atmospheric Chemistry and Physics, 7, 2103–2118, https://doi.org/10.5194/acp-7-2103-2007, 2007.

Boersma, K. F., Eskes, H. J., Dirksen, R. J., van der A, R. J., Veefkind, J. P., Stammes, P., Huijnen, V., Kleipool, Q. L., Sneep, M., Claas, J., Leitão, J., Richter, A., Zhou, Y., and Brunner, D.: An improved tropospheric NO_2 column retrieval algorithm for the Ozone Monitoring Instrument, Atmospheric Measurement Techniques, 4, 1905–1928, https://doi.org/10.5194/amt-4-1905-2011, 2011.

Boersma, K. F., Eskes, H. J., Richter, A., De Smedt, I., Lorente, A., Beirle, S., van Geffen, J. H. G. M., Zara, M., Peters, E., Van Roozendael, M., Wagner, T., Maasakkers, J. D., van der A, R. J., Nightingale, J., De Rudder, A., Irie, H., Pinardi, G., Lambert, J.-C., and Compernolle, S. C.: Improving algorithms and uncertainty estimates for satellite NO_2 retrievals: results from the quality assurance for the essential climate variables (QA4ECV) project, Atmospheric Measurement Techniques, 11, 6651–6678, https://doi.org/10.5194/amt-11-6651-2018, 2018.

Bovensmann, H., Burrows, J. P., Buchwitz, M., Frerick, J., Noël, S., Rozanov, V. V., Chance, K. V., and Goede, A. P. H.: SCIAMACHY: Mission objectives and measurement modes, Journal of the Atmospheric Sciences, 56, 127 – 150, https://doi.org/10.1175/1520-0469(1999)056<0127:SMOAMM>2.0.CO;2, 1999.

Bovensmann, H., Aben, I., Van Roozendael, M., Kühl, S., Gottwald, M., von Savigny, C., Buchwitz, M., Richter, A., Frankenberg, C., Stammes, P., de Graaf, M., Wittrock, F., Sinnhuber, M., Sinnhuber, B. M., Schönhardt, A., Beirle, S., Gloudemans, A., Schrijver, H., Bracher, A., Rozanov, A. V., Weber, M., and Burrows, J. P.: SCIAMACHY's view of the changing Earth's environment, in: SCIAMACHY - Exploring the changing Earth's atmosphere, edited by Gottwald, M. and Bovensmann, H., pp. 175–216, Springer Netherlands, Dordrecht, https://doi.org/10.1007/978-90-481-9896-2_10, 2011.

Box, G. E. P. and Cox, D. R.: An analysis of transformations, Journal of the Royal Statistical Society. Series B (Methodological), 26, 211–252, http://www.jstor.org/stable/2984418, 1964.

Bucsela, E., Celarier, E., Wenig, M., Gleason, J., Veefkind, J., Boersma, K., and Brinksma, E.: Algorithm for NO_2 vertical column retrieval from the Ozone Monitoring Instrument, IEEE Transactions on Geoscience and Remote Sensing, 44, 1245–1258, https://doi.org/10.1109/TGRS.2005.863715, 2006.

Bucsela, E. J., Krotkov, N. A., Celarier, E. A., Lamsal, L. N., Swartz, W. H., Bhartia, P. K., Boersma, K. F., Veefkind, J. P., Gleason, J. F., and Pickering, K. E.: A new stratospheric and tropospheric NO_2 retrieval algorithm for nadir-viewing satellite instruments: applications to OMI, Atmospheric Measurement Techniques, 6, 2607–2626, https://doi.org/10.5194/amt-6-2607-2013, 2013.

https://doi.org/10.5194/egusphere-2022-806
Preprint. Discussion started: 19 September 2022

Burrows, J. P., Weber, M., Buchwitz, M., Rozanov, V., Ladstätter-Weißenmayer, A., Richter, A., DeBeek, R., Hoogen, R., Bramstedt, K., Eichmann, K.-U., Eisinger, M., and Perner, D.: The Global Ozone Monitoring Experiment (GOME): Mission concept and first scientific results, Journal of the Atmospheric Sciences, 56, 151 – 175, https://doi.org/10.1175/1520-0469(1999)056<0151:TGOMEG>2.0.CO;2, 1999.

Choi, S., Lamsal, L. N., Follette-Cook, M., Joiner, J., Krotkov, N. A., Swartz, W. H., Pickering, K. E., Loughner, C. P., Appel, W., Pfister, G., Saide, P. E., Cohen, R. C., Weinheimer, A. J., and Herman, J. R.: Assessment of NO_2 observations during DISCOVER-AQ and KORUS-AQ field campaigns, Atmospheric Measurement Techniques, 13, 2523–2546, https://doi.org/10.5194/amt-13-2523-2020, 2020.

Cooper, M. J., Martin, R. V., Hammer, M. S., Levelt, P. F., Veefkind, P., Lamsal, L. N., Krotkov, N. A., Brook, J. R., and McLinden, C. A.: Global fine-scale changes in ambient NO_2 during COVID-19 lockdowns, Nature, 601, 380–387, https://doi.org/10.1038/s41586-021-04229-0, 2022.

Dobber, M.: OMI/Aura Level 1B UV Global Geolocated Earthshine Radiances 1-orbit L2 Swath 13x24 km V003, https://doi.org/10.5067/AURA/OMI/DATA1002, accessed: 25 October 2021, 2007a.

Dobber, M.: OMI/Aura Level 1B VIS Global Geolocated Earthshine Radiances 1-orbit L2 Swath 13x24 km V003, https://doi.org/10.5067/AURA/OMI/DATA1004, accessed: 25 October 2021, 2007b.

Duncan, B. N., Lamsal, L. N., Thompson, A. M., Yoshida, Y., Lu, Z., Streets, D. G., Hurwitz, M. M., and Pickering, K. E.: A space-based, high-resolution view of notable changes in urban NO_x pollution around the world (2005–2014), Journal of Geophysical Research: Atmospheres, 121, 976–996, https://doi.org/https://doi.org/10.1002/2015JD024121, 2016.

Fasnacht, Z., Vasilkov, A., Haffner, D., Qin, W., Joiner, J., Krotkov, N., Sayer, A. M., and Spurr, R.: A geometry-dependent surface Lambertian-equivalent reflectivity product for UV–Vis retrievals – Part 2: Evaluation over open ocean, Atmospheric Measurement Techniques, 12, 6749–6769, https://doi.org/10.5194/amt-12-6749-2019, 2019.

Fasnacht, Z., Joiner, J., Haffner, D., Qin, W., Vasilkov, A., Castellanos, P., and Krotkov, N.: Using machine learning for timely estimates of ocean color information from hyperspectral satellite measurements in the presence of clouds, aerosols, and sunglint, Frontier in Remote Sensing, 3, https://doi.org/10.3389/frsen.2022.846174, 2022.

Fleig, A. J., Bhartia, P. K., Wellemeyer, C. G., and Silberstein, D. S.: Seven years of total ozone from the TOMS instrument-A report on data quality, Geophysical Research Letters, 13, 1355–1358, https://doi.org/https://doi.org/10.1029/GL013i012p01355, 1986.

Goldberg, D. L., Anenberg, S. C., Kerr, G. H., Mohegh, A., Lu, Z., and Streets, D. G.: TROPOMI NO_2 in the United States: A detailed look at the annual averages, weekly cycles, effects of temperature, and correlation with surface NO_2 concentrations, Earth's Future, 9, e2020EF001 665–e2020EF001 665, https://doi.org/10.1029/2020EF001665, 2021.

Gorkavyi, N., Fasnacht, Z., Haffner, D., Marchenko, S., Joiner, J., and Vasilkov, A.: Detection of anomalies in the UV–vis reflectances from the Ozone Monitoring Instrument, Atmospheric Measurement Techniques, 14, 961–974, https://doi.org/10.5194/amt-14-961-2021, 2021.

Joiner, J. and Bhartia, P. K.: The determination of cloud pressures from rotational Raman scattering in satellite backscatter ultraviolet measurements, Journal of Geophysical Research: Atmospheres, 100, 23 019–23 026, https://doi.org/https://doi.org/10.1029/95JD02675, 1995.

Joiner, J., Fasnacht, Z., Qin, W., Yoshida, Y., Vasilkov, A. P., Li, C., Lamsal, L., and Krotkov, N.: Use of hyper-spectral visible and near-infrared satellite data for timely estimates of the Earth's surface reflectance in cloudy and aerosol loaded conditions: Part 1–Application to RGB image restoration over land with GOME-2, Frontiers in Remote Sensing, 2, https://doi.org/10.3389/frsen.2021.716430, 2022.

Judd, L. M., Al-Saadi, J. A., Szykman, J. J., Valin, L. C., Janz, S. J., Kowalewski, M. G., Eskes, H. J., Veefkind, J. P., Cede, A., Mueller, M., Gebetsberger, M., Swap, R., Pierce, R. B., Nowlan, C. R., Abad, G. G., Nehrir, A., and Williams, D.: Evaluating Sentinel-5P TROPOMI

https://doi.org/10.5194/egusphere-2022-806
Preprint. Discussion started: 19 September 2022

tropospheric NO_2 column densities with airborne and Pandora spectrometers near New York City and Long Island Sound, Atmospheric Measurement Techniques, 13, 6113–6140, https://doi.org/10.5194/amt-13-6113-2020, 2020.

Kerr, G. H., Goldberg, D. L., and Anenberg, S. C.: COVID-19 pandemic reveals persistent disparities in nitrogen dioxide pollution, Proceedings of the National Academy of Sciences, 118, e2022409 118, https://doi.org/10.1073/pnas.2022409118, 2021.

Krotkov, N. A., McLinden, C. A., Li, C., Lamsal, L. N., Celarier, E. A., Marchenko, S. V., Swartz, W. H., Bucsela, E. J., Joiner, J., Duncan, B. N., Boersma, K. F., Veefkind, J. P., Levelt, P. F., Fioletov, V. E., Dickerson, R. R., He, H., Lu, Z., and Streets, D. G.: Aura OMI observations of regional SO_2 and NO_2 pollution changes from 2005 to 2015, Atmospheric Chemistry and Physics, 16, 4605–4629, https://doi.org/10.5194/acp-16-4605-2016, 2016.

Krotkov, N. A., Lamsal, L. N., Marchenko, S. V., J.Bucsela, E., Swartz, W. H., Joiner, J., and the OMI core team: OMI/Aura Nitrogen dioxide (NO_2) total and Tropospheric Column 1-orbit L2 Swath 13x24 km V003, https://doi.org/10.5067/Aura/OMI/DATA2017, accessed: 25 October 2021, 2019.

Lamsal, L. N., Krotkov, N. A., Celarier, E. A., Swartz, W. H., Pickering, K. E., Bucsela, E. J., Gleason, J. F., Martin, R. V., Philip, S., Irie, H., Cede, A., Herman, J., Weinheimer, A., Szykman, J. J., and Knepp, T. N.: Evaluation of OMI operational standard NO_2 column retrievals using in situ and surface-based NO_2 observations, Atmospheric Chemistry and Physics, 14, 11 587–11 609, https://doi.org/10.5194/acp-14-11587-2014, 2014.

Lamsal, L. N., Duncan, B. N., Yoshida, Y., Krotkov, N. A., Pickering, K. E., Streets, D. G., and Lu, Z.: U.S. NO_2 trends (2005–2013): EPA Air Quality System (AQS) data versus improved observations from the Ozone Monitoring Instrument (OMI), Atmospheric Environment, 110, 130–143, https://doi.org/https://doi.org/10.1016/j.atmosenv.2015.03.055, 2015.

Lamsal, L. N., Krotkov, N. A., Vasilkov, A., Marchenko, S., Qin, W., Yang, E.-S., Fasnacht, Z., Joiner, J., Choi, S., Haffner, D., Swartz, W. H., Fisher, B., and Bucsela, E.: Ozone Monitoring Instrument (OMI) Aura nitrogen dioxide standard product version 4.0 with improved surface and cloud treatments, Atmospheric Measurement Techniques, 14, 455–479, https://doi.org/10.5194/amt-14-455-2021, 2021.

Lary, D. J., Alavi, A. H., Gandomi, A. H., and Walker, A. L.: Machine learning in geosciences and remote sensing, Geoscience Frontiers, 7, 3–10, https://doi.org/https://doi.org/10.1016/j.gsf.2015.07.003, special Issue: Progress of Machine Learning in Geosciences, 2016.

Le, C. and Hu, C.: A hybrid approach to estimate chromophoric dissolved organic matter in turbid estuaries from satellite measurements: A case study for Tampa Bay, Opt. Express, 21, 18 849–18 871, https://doi.org/10.1364/OE.21.018849, 2013.

Lerot, C., Stavrakou, T., De Smedt, I., Müller, J.-F., and Van Roozendael, M.: Glyoxal vertical columns from GOME-2 backscattered light measurements and comparisons with a global model, Atmospheric Chemistry and Physics, 10, 12 059–12 072, https://doi.org/10.5194/acp-10-12059-2010, 2010.

Levelt, P., van den Oord, G., Dobber, M., Malkki, A., Visser, H., de Vries, J., Stammes, P., Lundell, J., and Saari, H.: The ozone monitoring instrument, IEEE Transactions on Geoscience and Remote Sensing, 44, 1093–1101, https://doi.org/10.1109/TGRS.2006.872333, 2006.

Levelt, P. F., Joiner, J., Tamminen, J., Veefkind, J. P., Bhartia, P. K., Stein Zweers, D. C., Duncan, B. N., Streets, D. G., Eskes, H., van der A, R., McLinden, C., Fioletov, V., Carn, S., de Laat, J., DeLand, M., Marchenko, S., McPeters, R., Ziemke, J., Fu, D., Liu, X., Pickering, K., Apituley, A., González Abad, G., Arola, A., Boersma, F., Chan Miller, C., Chance, K., de Graaf, M., Hakkarainen, J., Hassinen, S., Ialongo, I., Kleipool, Q., Krotkov, N., Li, C., Lamsal, L., Newman, P., Nowlan, C., Suleiman, R., Tilstra, L. G., Torres, O., Wang, H., and Wargan, K.: The Ozone Monitoring Instrument: Overview of 14 years in space, Atmospheric Chemistry and Physics, 18, 5699–5745, https://doi.org/10.5194/acp-18-5699-2018, 2018.

https://doi.org/10.5194/egusphere-2022-806
Preprint. Discussion started: 19 September 2022

Li, C., Xu, X., Liu, X., Wang, J., Sun, K., van Geffen, J., Zhu, Q., Ma, J., Jin, J., Qin, K., He, Q., Xie, P., Ren, B., and Cohen, R. C.: Direct retrieval of NO_2 vertical columns from UV-Vis (390-495 nm) spectral radiances using a neural network, Journal of Remote Sensing, 2022, 9817 134, https://doi.org/10.34133/2022/9817134, 2022.

Liu, F., Tao, Z., Beirle, S., Joiner, J., Yoshida, Y., Smith, S. J., Knowland, K. E., and Wagner, T.: A new method for inferring city emissions and lifetimes of nitrogen oxides from high-resolution nitrogen dioxide observations: a model study, Atmospheric Chemistry and Physics, 22, 1333–1349, https://doi.org/10.5194/acp-22-1333-2022, 2022.

Mannino, A., Russ, M. E., and Hooker, S. B.: Algorithm development and validation for satellite-derived distributions of DOC and CDOM in the U.S. Middle Atlantic Bight, Journal of Geophysical Research: Oceans, 113, https://doi.org/10.1029/2007JC004493, 2008.

Marchenko, S., Krotkov, N. A., Lamsal, L. N., Celarier, E. A., Swartz, W. H., and Bucsela, E. J.: Revising the slant column density retrieval of nitrogen dioxide observed by the Ozone Monitoring Instrument, Journal of Geophysical Research: Atmospheres, 120, 5670–5692, https://doi.org/10.1002/2014JD022913, 2015.

Maxwell, A. E., Warner, T. A., and Fang, F.: Implementation of machine-learning classification in remote sensing: an applied review, International Journal of Remote Sensing, 39, 2784–2817, https://doi.org/10.1080/01431161.2018.1433343, 2018.

Munro, R., Lang, R., Klaes, D., Poli, G., Retscher, C., Lindstrot, R., Huckle, R., Lacan, A., Grzegorski, M., Holdak, A., Kokhanovsky, A., Livschitz, J., and Eisinger, M.: The GOME-2 instrument on the Metop series of satellites: instrument design, calibration, and level 1 data processing – an overview, Atmospheric Measurement Techniques, 9, 1279–1301, https://doi.org/10.5194/amt-9-1279-2016, 2016.

NASA: NASA targets coastal ecosystems with new space sensor, https://www.nasa.gov/press-release/nasa-targets-coastal-ecosystems-with-new-space-sensor, RELEASE 19-065, 2019.

Noxon, J. F.: Nitrogen dioxide in the stratosphere and troposphere measured by ground-based absorption spectroscopy, Science, 189, 547–549, https://doi.org/10.1126/science.189.4202.547, 1975.

Platt, U.: Differential optical absorption spectroscopy (DOAS), in: Air Monitoring by Spectrometric Techniques, volume 127 of Chemical Analysis Series, edited by Sigrist, M. W., p. 27–84, John Wiley, New York, USA, 1994.

Platt, U. and Perner, D.: Measurements of atmospheric trace gases by long path differential UV/visible absorption spectroscopy, in: Optical and Laser Remote Sensing, edited by Killinger, D. A. and Mooradien, A., p. 95–105, Springer Verlag, New York, USA, 1983.

Platt, U. and Stutz, J.: in: Differential Optical Absorption Spectroscopy (DOAS), Principle and Applications, Springer Verlag, Heidelberg, 2006.

Qin, W., Fasnacht, Z., Haffner, D., Vasilkov, A., Joiner, J., Krotkov, N., Fisher, B., and Spurr, R.: A geometry-dependent surface Lambertian-equivalent reflectivity product for UV–Vis retrievals – Part 1: Evaluation over land surfaces using measurements from OMI at 466 nm, Atmospheric Measurement Techniques, 12, 3997–4017, https://doi.org/10.5194/amt-12-3997-2019, 2019.

Richter, A. and Burrows, J.: Tropospheric NO_2 from GOME measurements, Advances in Space Research, 29, 1673–1683, https://doi.org/10.1016/S0273-1177(02)00100-X, 2002.

Richter, A., Begoin, M., Hilboll, A., and Burrows, J. P.: An improved NO_2 retrieval for the GOME-2 satellite instrument, Atmospheric Measurement Techniques, 4, 1147–1159, https://doi.org/10.5194/amt-4-1147-2011, 2011.

Richter, A., Hilboll, A., and Burrows, J. P.: A multi-wavelength retrieval of tropospheric NO_2 from GOME-2 , http://www.iup.uni-bremen.de/doas/posters/dpg_2014_richter.pdf, dPG Spring Meeting, Berlin, Germany, 2014.

Schmidhuber, J.: Deep learning in neural networks: An overview, Neural Networks, 61, 85–117, https://doi.org/https://doi.org/10.1016/j.neunet.2014.09.003, 2015.

https://doi.org/10.5194/egusphere-2022-806
Preprint. Discussion started: 19 September 2022

Shindell, D. T., Faluvegi, G., Koch, D. M., Schmidt, G. A., Unger, N., and Bauer, S. E.: Improved attribution of climate forcing to emissions, Science, 326, 716–718, https://doi.org/10.1126/science.1174760, 2009.

Tzortziou, M., Herman, J. R., Ahmad, Z., Loughner, C. P., Abuhassan, N., and Cede, A.: Atmospheric NO_2 dynamics and impact on ocean color retrievals in urban nearshore regions, Journal of Geophysical Research: Oceans, 119, 3834–3854, https://doi.org/10.1002/2014JC009803, 2014.

Valks, P., Pinardi, G., Richter, A., Lambert, J.-C., Hao, N., Loyola, D., Van Roozendael, M., and Emmadi, S.: Operational total and tropospheric NO_2 column retrieval for GOME-2, Atmospheric Measurement Techniques, 4, 1491–1514, https://doi.org/10.5194/amt-4-1491-2011, 2011.

van Geffen, J., Boersma, K. F., Eskes, H., Sneep, M., ter Linden, M., Zara, M., and Veefkind, J. P.: S5P TROPOMI NO_2 slant column retrieval: method, stability, uncertainties and comparisons with OMI, Atmospheric Measurement Techniques, 13, 1315–1335, https://doi.org/10.5194/amt-13-1315-2020, 2020.

van Geffen, J. H. G. M., Boersma, K. F., Van Roozendael, M., Hendrick, F., Mahieu, E., De Smedt, I., Sneep, M., and Veefkind, J. P.: Improved spectral fitting of nitrogen dioxide from OMI in the 405–465 nm window, Atmospheric Measurement Techniques, 8, 1685–1699, https://doi.org/10.5194/amt-8-1685-2015, 2015.

Vandaele, A. C., Hermans, C., Simon, P. C., Carleer, M. R., Colin, R., Fally, S., Merienne, M. F., Jenouvrier, A., and Coquart, B.: Measurements of the NO_2 absorption cross-section from 42,000 cm^{-1} to 10,000 cm^{-1} (238–1000 nm) at 220 K and 294 K, Journal of Quantitative Spectroscopy and Radiative Transfer, 59, 171–184, 1998.

Vasilkov, A., Qin, W., Krotkov, N., Lamsal, L., Spurr, R., Haffner, D., Joiner, J., Yang, E.-S., and Marchenko, S.: Accounting for the effects of surface BRDF on satellite cloud and trace-gas retrievals: A new approach based on geometry-dependent Lambertian equivalent reflectivity applied to OMI algorithms, Atmospheric Measurement Techniques, 10, 333–349, https://doi.org/10.5194/amt-10-333-2017, 2017.

Vasilkov, A., Yang, E.-S., Marchenko, S., Qin, W., Lamsal, L., Joiner, J., Krotkov, N., Haffner, D., Bhartia, P. K., and Spurr, R.: A cloud algorithm based on the O_2–O_2 477 nm absorption band featuring an advanced spectral fitting method and the use of surface geometry-dependent Lambertian-equivalent reflectivity, Atmospheric Measurement Techniques, 11, 4093–4107, https://doi.org/10.5194/amt-11-4093-2018, 2018.

Veefkind, J., Aben, I., McMullan, K., Förster, H., de Vries, J., Otter, G., Claas, J., Eskes, H., de Haan, J., Kleipool, Q., van Weele, M., Hasekamp, O., Hoogeveen, R., Landgraf, J., Snel, R., Tol, P., Ingmann, P., Voors, R., Kruizinga, B., Vink, R., Visser, H., and Levelt, P.: TROPOMI on the ESA Sentinel-5 Precursor: A GMES mission for global observations of the atmospheric composition for climate, air quality and ozone layer applications, Remote Sensing of Environment, 120, 70 – 83, https://doi.org/https://doi.org/10.1016/j.rse.2011.09.027, the Sentinel Missions - New Opportunities for Science, 2012.

Yang, K., Carn, S. A., Ge, C., Wang, J., and Dickerson, R. R.: Advancing measurements of tropospheric NO_2 from space: New algorithm and first global results from OMPS, Geophysical Research Letters, 41, 4777–4786, https://doi.org/https://doi.org/10.1002/2014GL060136, 2014.

Zoogman, P., Liu, X., Suleiman, R. M., Pennington, W. F., Flittner, D. E., Al-Saadi, J. A., Hilton, B. B., Nicks, D. K., Newchurch, M. J., Carr, J. L., Janz, S. J., Andraschko, M. R., Arola, A., Baker, B. D., Canova, B. P., Miller, C. C., Cohen, R. C., Davis, J. E., Dussault, M. E., Edwards, D. P., Fishman, J., Ghulam, A., Abad, G. G., Grutter, M., Herman, J. R., Houck, J., Jacob, D. J., Joiner, J., Kerridge, B. J., Kim, J., Krotkov, N. A., Lamsal, L., Li, C., Lindfors, A., Martin, R. V., McElroy, C. T., McLinden, C., Natraj, V., Neil, D. O., Nowlan, C. R., O'Sullivan, E. J., Palmer, P. I., Pierce, R. B., Pippin, M. R., Saiz-Lopez, A., Spurr, R. J. D., Szykman, J. J., Torres, O., Veefkind, J. P.,

https://doi.org/10.5194/egusphere-2022-806
Preprint. Discussion started: 19 September 2022

Veihelmann, B., Wang, H., Wang, J., and Chance, K.: Tropospheric emissions: Monitoring of pollution (TEMPO), Journal of Quantitative Spectroscopy and Radiative Transfer, 186, 17 – 39, https://doi.org/http://dx.doi.org/10.1016/j.jqsrt.2016.05.008, 2017.